Exploiting Inter-Sample Information for Long-tailed Out-of-Distribution Detection

Nimeshika Udayangani, Hadi M. Dolatabadi, Sarah Erfani, and Christopher Leckie The University of Melbourne

{nhewadehigah@student., h.dolatabadi@, sarah.erfani@, caleckie@}unimelb.edu.au

Abstract

Detecting out-of-distribution (OOD) data is essential for safe deployment of deep neural networks (DNNs). This problem becomes particularly challenging in the presence of long-tailed in-distribution (ID) datasets, often leading to high false positive rates (FPR) and low tail-class ID classification accuracy. In this paper, we demonstrate that exploiting inter-sample relationships using a graph-based representation can significantly improve OOD detection in long-tailed recognition of vision datasets. To this end, we use the feature space of a pre-trained model to initialize our graph structure. We account for the differences between the activation layer distribution of the pre-training vs. training data, and actively introduce Gaussianization to alleviate any deviations from a standard normal distribution in the activation layers of the pre-trained model. We then refine this initial graph representation using graph convolutional networks (GCNs) to arrive at a feature space suitable for long-tailed OOD detection. This leads us to address the inferior performance observed in ID tail-classes within existing OOD detection methods. Experiments over three benchmarks CIFAR10-LT, CIFAR100-LT, and ImageNet-LT demonstrate that our method outperforms the state-of-theart approaches by a large margin in terms of FPR and tailclass ID classification accuracy.

1. Introduction

Deep neural networks (DNNs) exhibit remarkable performance provided that the data encountered during testing closely aligns with the data used for training. However, when DNN models encounter samples that are different from their training distribution (a.k.a., out-of-distribution (OOD) samples), they often assign overly confident predictions even when a distribution mismatch exists [31]. As a consequence, ensuring safe deployment of these models in critical domains, such as healthcare [45] and autonomous driving [9], necessitates methods that can

reliably detect OOD samples.

There have been numerous methods proposed to detect OOD samples showing promising results [7, 12, 15, 24, 25, 36]. However, most of these methods are commonly assessed using balanced class in-distributions (IDs), which does not reflect real-world scenarios where the training data often exhibits a long-tailed (LT) distribution. In a long-tailed distribution, a few dominant classes have a large number of samples (head-classes), while the remaining classes (tail-classes) have relatively fewer samples. As a result, models find it difficult to distinguish tail-class ID samples from OOD samples when compared to head-class ID samples. This leads to a high false positive rate (FPR) for OOD detection and low tail-class ID classification accuracy in current methods, thereby making OOD detection extremely challenging [39]. It was not until very recently that Wang et al. [39] formally introduced the problem of OOD detection in long-tailed recognition (LTR) for the first time. Following this trend, a few other methods [3, 27, 42] evaluated their models on long-tailed training sets.

However, a common approach with these OOD detection methods — as well as previous methods using balanced IDs — is that they treat each sample individually during training, overlooking the interconnected relationships within the data. We instead propose to exploit the inter-sample relationships within both ID and OOD data to address the more challenging problem of OOD detection in long-tailed settings. With the help of this additional relationship information, we aim to enhance the distinguishability of tail samples. To this end, we transform image datasets into graph-based representations, allowing us to utilize the full structure underlying the data.

In particular, we first use the feature space of a pretrained model to initialize a graph structure using k nearest neighbor (k-NN) graphs. Even though there have been traces of pre-training being utilized to improve OOD detection [7, 13, 14], none of these studies specifically explore the presence of long-tailed IDs. DNNs are unable to learn discriminative representations of tail-classes due to the scarcity of their training samples. Pre-training can

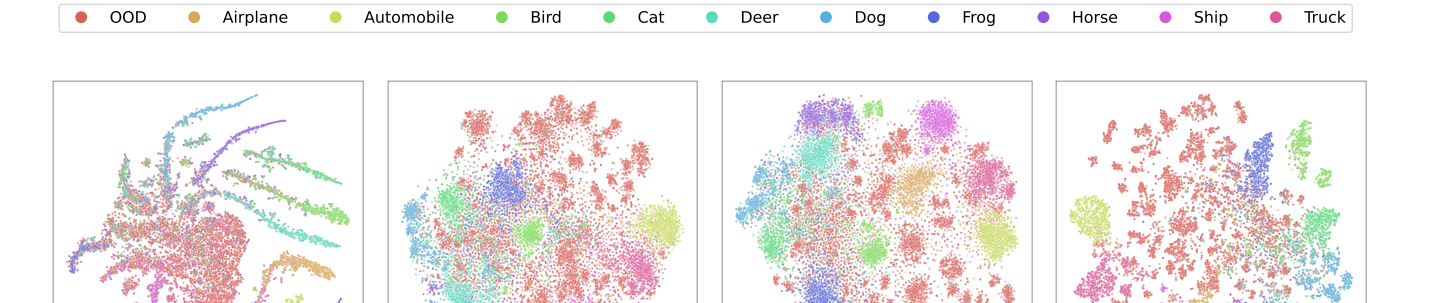


Figure 1. Feature space representations of CIFAR10-LT as ID test set and CIFAR-100 as OOD test set using t-SNE. (a) Feature distribution of ResNet18 trained from scratch using OE [15], (b) ResNet18 pre-trained on Downsampled ImageNet, (c) same model in (b) after applying Gaussianization, and (d) model in (c) after message passing using GCN. Tail ID classes (*e.g.*, Horse, Ship, Truck) heavily overlap with OOD samples (represented as red dots) in (a). Separability enhanced from left to right, wherein (d) there are clear gaps between the

(b) Pre-trained.

alleviate this problem by exploiting prior knowledge from additional datasets, which can help to characterize the tail-classes. Due to the large-scale nature of these datasets, they often contain a variety of different samples, thus helping to achieve a more balanced performance when transferred to the long-tailed data. These ensure meaningful initial feature embeddings for our intended downstream task. As shown for the CIFAR10-LT dataset in Fig. 1, feature space representations from a pre-trained model (Fig. 1b) facilitate a better separability among OOD and ID samples compared to a model trained from scratch (Fig. 1a) using Outlier Exposure (OE) [15].

(a) Scratch trained OE.

decision boundaries.

To further improve the quality of our initial representations, we account for the distributional differences between the activation layer of the pre-training vs. training data. A recent study [19] highlights the significance of ensuring that the activation layer representations of data adhere to a standard normal distribution. To address this issue, we actively introduce Gaussianization to alleviate any deviations from a standard normal distribution in the activation layers of the pre-trained model during feature extraction (Fig. 1c). In this step, we update the batch norm [18] statistics of the pretrained model to align it with our long-tailed distribution. Finally, we refine this initial graph representation using message passing in the form of graph convolutional networks (GCNs) to arrive at a feature space suitable for longtailed OOD detection (Fig. 1d). To the best of our knowledge, we are the first to exploit inter-sample information to address the problem of long-tailed OOD detection in the vision domain. In summary, our contributions are as follows:

 We improve the tail-class representations utilizing inter-sample relationships by proposing a graph-based solution for OOD detection in long-tailed recognition. We demonstrate that applying Gaussianization to the activation layers of the pre-trained model, using an auxiliary dataset to represent OOD data, can further improve the overall performance

(d) After GCN

• Our method outperforms the SOTA by a large margin; (12.55%, 8.51%) FPR and (10.64%, 12.95%) tail-class ID classification accuracy on CIFAR10-LT and CIFAR100-LT, respectively. We also demonstrate our method can improve the performance on large-scale OOD detection tasks using ImageNet-LT.

2. Related work

(c) Pre-trained after Gaussianization.

This section provides a brief overview of SOTA methods alongside baseline approaches, laying the groundwork for our research around OOD detection in LTR. We also delve into the significance of pre-training for OOD detection and explore the application of graph-based techniques for handling arbitrary data within our study.

2.1. OOD detection

Hendrycks and Gimpel [12] first suggested a baseline approach for identifying OOD samples using the maximum softmax probability (MSP) from DNNs. This work revealed that OOD samples consistently exhibit lower MSP values compared to ID samples. Similarly, to detect OOD samples other methods suggested different confidence scores (e.g., Mahalanobis distance [24], and Gram matrix values [34]) which can be applied to any pre-trained network. Very recently, KNN [36] suggested non-parametric nearestneighbour distance for OOD detection. While both our method and KNN employ k-NN, the usage is different. It utilizes k-NN as an OOD score, whereas we employ k-NN

to establish our graph structure. Moreover, our method distinguishes itself from KNN by incorporating graph representations to leverage inter-sample relationships.

Another set of approaches [15, 20, 25, 32] aim to leverage auxiliary datasets of outliers to improve the OOD detection. Rather than training solely on ID data, these approaches exposed DNNs to OOD examples. Outlier Exposure (OE) [15] modified the loss function of classification tasks by adding the KL divergence between the model's outputs for these training OOD samples and the uniform distribution. This modification led to improved performance compared to models trained exclusively on ID data. Following this method, EnergyOE [25] and CFL [20] used an energy score to differentiate between the auxiliary OOD samples and ID samples. Then, OECC [32] proposed to minimize the total variation distance between the distributions instead of the KL divergence metric. While these works propose promising solutions for OOD detection, their applicability is limited to datasets with a relatively balanced distribution.

2.2. Long-tailed OOD detection

Despite the significant progress in OOD detection methods, very limited attention has been drawn to long-tailed IDs. PASCL [39] was the first to demonstrate the significant challenges of OOD detection in LTR and showed that this problem cannot be addressed by naïvely combining SOTA OOD detection methods with long-tailed recognition methods. As a solution, PASCL applies supervised contrastive learning partially and asymmetrically to explicitly distinguish tail-class ID samples from OOD samples. Recently, Balanced-EnergyOE (BE-OE) [3] updated the loss function of OE by introducing a balanced energy regularization loss, while OS [41] assigned noisy labels to unlabeled OE data to re-balance the class priors in the training dataset. However, these methods require fitting a prior distribution of OE data to ID data, which is difficult in LTR. To address this, COCL [27] and EAT [42] introduced abstention classes to better encapsulate the OOD samples and achieved SOTA results for OOD detection in LTR. Different from all these methods, our method is designed to exploit inter-sample information by means of graph representation learning to improve OOD detection.

2.3. Pre-training for OOD detection

Zeiler and Fergus [47] found that a pre-trained network on the ImageNet dataset [33] can generalize well to other datasets, achieving a remarkable classification performance even with very limited numbers of training samples. Apart from classification tasks, Hendrycks *et al.* [13] showed that pre-training can improve OOD detection on image datasets. They also demonstrated that certain properties, including the model's robustness to class imbalance, can be improved

by pre-training. Similarly, pre-trained transformers have been shown to improve OOD detection in the domain of natural language processing [14]. Following this, Fort *et al.* [7] showed that a pre-trained Vision Transformer (ViT) can improve OOD detection in vision benchmarks. They also introduced few-shot OE to further improve OOD detection assuming that a few labelled samples from the test OOD dataset are available during training time. Similarly, self-supervised pre-training has also been shown to improve OOD detection [16, 29]. However, none of these studies has examined how pre-training can improve OOD detection in the presence of long-tailed IDs. We are the first to incorporate pre-training to improve OOD detection in LTR.

2.4. Graph neural networks for arbitrary data

Following the concept of CNNs, GCNs [21] enable the generalization of neural network models to datasets structured as graphs. In terms of message passing [8], GCN can capture complex relationships and inter-dependencies among nodes in a graph. Since many modalities can be organized as graphs, GCNs made their way into the domain of computer vision [6, 28, 38, 40, 44, 48]. Zhang et al. [48] deployed GCN for label noise cleansing in facial recognition tasks. Several other studies [6, 40, 44] employed GCN for face image clustering. The idea of GraphSAGE [10] was leveraged for tasks like image classification in CNN2Graph [38] and image retrieval in [28]. In this paper, however, we explore the introduction of GCN into the field of OOD detection in vision datasets. To the best of our knowledge, this is the first work that harnesses GCN to improve OOD detection alongside LTR.

3. Proposed method

In this section, we propose our approach, which aims to improve the distinguishability of tail classes from OOD data by leveraging inter-sample relationships. To achieve this, we use graph representation learning to transform the input dataset into graph-based representations. We followed two important design choices to enhance the initial representations. First, we apply pre-training to obtain less biased feature representations. Next, we use Gaussianization to ensure that the activation layer representations conform to a standard normal distribution. Finally, we refine this initial graph representation using GCN, to arrive at a feature space suitable for long-tailed OOD detection.

We begin by providing a formal definition of our problem statement in Sec. 3.1. Then, we describe each of the three major components that form the foundation of our methodology, as illustrated in Fig. 2: (i) graph representation learning (Sec. 3.2), (ii) pre-training (Sec. 3.3), and (iii) Gaussianization of pre-trained activation layers (Sec. 3.4).

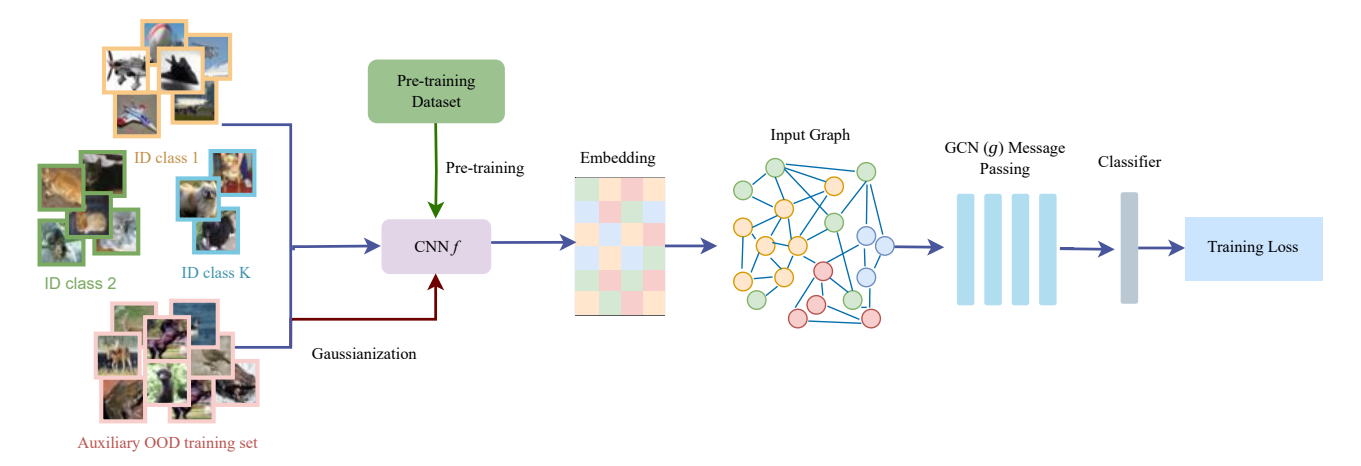


Figure 2. Overview of proposed methodology. Given \mathcal{D}_{in} with K classes and an auxiliary OOD training set \mathcal{D}_{out}^{OE} , we extract the initial feature embeddings from a pre-trained backbone model f after applying Gaussianization using the same training data. We then create a k-NN graph to refine these initial features using message passing in the form of GCN g. Then, we incorporate a fully-connected classifier to arrive at the objective loss for training g.

3.1. Problem statement

Let us consider a deep neural network model f. To train such models, we usually assume we have access to samples coming from a distribution referred to as $\mathcal{D}_{\mathrm{in}}$ (in**distribution**) (ID), consisting of $(x_{\rm in}, y_{\rm in})$ pairs. Here, $x_{\rm in}$ denotes the ID input image, and $y_{in} \in \mathcal{Y}_{in} := \{1, ..., K\}$ denotes its class label. The term **out-of-distribution** (OOD) detection usually refers to identifying samples x_{out} that do not belong to $\mathcal{D}_{\mathrm{in}}$ and their label set has no intersection with $\mathcal{Y}_{\mathrm{in}}.$ We denote this distribution as $\mathcal{D}_{\mathrm{out}}.$ In our case, the ID data $\mathcal{D}_{\mathrm{in}}$ has a long-tailed distribution. Without loss of generality, we assume that this distribution is characterized by an exponential decay in sample sizes across different classes with an imbalance ratio ρ , which denotes the ratio between sample sizes of the most frequent and least frequent classes. In other words, we assume $\hat{\rho} = \max_i \{n_i\} / \min_i \{n_i\}$ where $\{n_i\}_{i=1}^K$ represents the sample sizes for different classes.

In this problem setting, we aim to train neural networks f such that they can: (i) correctly distinguish OOD samples $\boldsymbol{x}_{\text{out}}$ from ID samples $\boldsymbol{x}_{\text{in}}$, and (ii) classify ID samples into one of the K classes with a competitive accuracy for the less common "tail-classes" as those for the more prevalent "head-classes". We can formulate our training objective as

$$\mathcal{L} = \mathbb{E}_{(\boldsymbol{x}_{\text{in}}, y_{\text{in}}) \sim \mathcal{D}_{\text{in}}} \left[\mathcal{L}_{\text{in}}(f(\boldsymbol{x}_{\text{in}}), y_{\text{in}}) \right] + \lambda \mathbb{E}_{\boldsymbol{x}_{\text{out}} \sim \mathcal{D}_{\text{out}}} \left[\mathcal{L}_{\text{out}}(f(\boldsymbol{x}_{\text{out}})) \right], \quad (1)$$

where $\mathcal{L}_{\rm in}$ is a loss function used for ID classification, and $\mathcal{L}_{\rm out}$ aims to satisfy our objective over OOD data. Since we assume a realistic scenario where we have no prior knowledge of test-time OOD data during training, we use Outlier Exposure (OE) [15] and introduce an auxiliary dataset $\mathcal{D}_{\rm out}^{\rm OE}$ that is entirely disjoint from test-time OOD data $\mathcal{D}_{\rm out}^{\rm test}$. Us-

ing maximum softmax probability as the OOD score [12], $\mathcal{L}_{\rm in}$ in Eq. (1) takes the form of cross-entropy loss, and $\mathcal{L}_{\rm out}$ can be defined as the KL divergence between the model's output and the uniform distribution \mathcal{U} :

$$\mathcal{L} = \mathbb{E}_{(\boldsymbol{x}_{\text{in}}, y_{\text{in}}) \sim \mathcal{D}_{\text{in}}} \left[\mathcal{L}_{\text{CE}}(f(\boldsymbol{x}_{\text{in}}), y_{\text{in}}) \right] + \lambda \mathbb{E}_{\boldsymbol{x}_{\text{out}} \sim \mathcal{D}_{\text{out}}^{\text{OE}}} \left[\text{KL}(f(\boldsymbol{x}_{\text{out}}) \parallel \mathcal{U}) \right].$$
(2)

3.2. Graph representation learning

As mentioned in Sec. 1, we want to have a training process that is fully aware of the overall structure underlying our dataset. Intuitively, we aim to ensure that the tail-class ID samples are not dominated by both the head-classes and the OOD samples. To materialize this in the form of an inductive bias, we resort to organizing our input dataset using a graph structure. This way, we aim to improve the OOD detection in the presence of tail-classes by leveraging the inter-sample relationships within the data. Existing OOD detection methods [3, 15, 39] only consider relationships between pairs or triplets of samples, or treat each sample completely individually to take the embedding space of the data. These methods, however, do not explore the embedding space in its entirety [35]. To address this, we create a graph using all images in the training dataset to capture the relationships among all samples and apply message passing in the form of GCN [21].

More precisely, we refine embeddings from a backbone CNN f using a GCN model g to obtain a more rectified embedding representation $z=g\left(f\left(x\right)\right)$ before proceeding with the loss calculation in Eq. (2). Let \mathcal{X} denote the matrix of initial embeddings (the selection of initial embeddings is discussed further in the next section) from f for all samples in the training dataset $(\{\mathcal{D}_{\text{in}} \cup \mathcal{D}_{\text{out}}^{\text{OE}}\})$. We calculate the pairwise cosine similarity $S=\mathcal{X}\mathcal{X}^T$ to build a k-nearest

neighbors (k-NN) undirected graph $\mathcal{G} = (\mathcal{X}, A)$ where A represents the adjacency matrix. If we consider the GCN operator from [21], then the layer-wise forward propagation rule of g is given by:

$$H^{(l+1)} = \sigma \left(\tilde{D}^{-\frac{1}{2}} \tilde{A} \tilde{D}^{-\frac{1}{2}} H^{(l)} W^{(l)} \right), \tag{3}$$

where $\tilde{A}=A+I_N$, and I_N is the identity matrix. Also, we define $\tilde{D}_{ii}=\sum_j \tilde{A}_{ij}$ and $W^{(l)}$ is a trainable weight matrix in the l^{th} layer. Finally, $H^{(l)}$ is the l^{th} layer output matrix, with $H^{(0)}=\mathcal{X}$, and σ denotes the activation function.

Instead of a CNN, which only considers intra-image local neighborhoods to calculate the feature representation of a sample, the GCN enables construction of an interimage feature representation that aggregates neighboring information from multiple images. This additional relational information helps refine the poor representations of tail-class ID samples, as shown in Fig. 1d, resulting in a more significant margin between the decision boundary of tail-class ID and OOD samples.

It should be noted that we construct graphs in an inductive setting, where test data is not available to the training graph and the model can make inferences across different test graphs consisting of samples from \mathcal{D}_{in}^{test} and \mathcal{D}_{out}^{test} .

3.3. Pre-training

The selection of the initial feature embeddings vector \mathcal{X} is very important, as this will decide the overall structure underlying the input graph for the subsequent message passing and feature refinement process. One can choose a DNN model trained from scratch as the backbone network f above to extract the initial embeddings \mathcal{X} . However, such an embedding distribution may be sub-optimal as the trained model is still biased towards the prevalent classes providing a poor prior for the downstream task.

It is well-known that pre-training is useful in leveraging the knowledge learned from a large, diverse dataset for specific tasks with limited data [47]. In our case, we have very limited tail-class ID samples, thus, it is conceivable that pre-training can be used to improve their representations. Figure 1 illustrates this fact by showing improved discrimination between the tail classes and OOD samples in the initial feature embedding space of a pre-trained model (Fig. 1b) compared to a model trained from scratch (Fig. 1a). Therefore, we use a model pre-trained on a large dataset that is independent from $\mathcal{D}_{\rm in}, \mathcal{D}_{\rm out}^{\rm OE}$, and $\mathcal{D}_{\rm out}^{\rm test}$ to generate \mathcal{X} .

3.4. Gaussianization of pre-trained activation layers

Regularization and normalization techniques are commonly applied to neural networks. A recent study [19] highlights the significance of ensuring that the activation layer representations of data adhere to a standard normal distribution. However, when we forward pass our training

datasets through a DNN that has been pre-trained on a different dataset, this can lead to a misalignment of the activation layers from the intended standard normal distribution. To rectify this misalignment, we apply Gaussianization to adjust the sample mean and sample variance of each activation layer of the pre-trained network to match those of the new training data, ensuring that their activations conform to a standard normal distribution. Accordingly, before extracting $\mathcal X$ from the pre-trained model f, we update its batch normalization (BN) [18] statistics by fine-tuning it for an additional set of epochs on all the training data. Feature space representation after this process (Fig. 1c) is substantially improved compared to the original one (Fig. 1b).

4. Evaluation

In this section, we evaluate the performance of our proposed model in terms of (i) OOD detection, and (ii) ID classification. We describe the experimental settings that we used. Our results demonstrate the effectiveness of our approach in comparison with the baselines, achieving SOTA performance in all settings. Additionally, we conduct thorough ablation studies to demonstrate the effectiveness of each component of our method.

4.1. Experimental settings

ID datasets ($\mathcal{D}_{\rm in}$, $\mathcal{D}_{\rm in}^{\rm test}$): We use three long-tailed datasets, CIFAR10-LT, CIFAR100-LT [1] with the imbalance ratio $\rho=100$ following [27,39,42], and ImageNet-LT [26] as ID data. As $\mathcal{D}_{\rm in}^{\rm test}$, we use balanced test sets of the original CIFAR datasets [22] and the validation set of ImageNet [33]. **OE** datasets ($\mathcal{D}_{\rm out}^{\rm OE}$): We use two auxiliary datasets, 80 Million Tiny Images [37] in the case of training over CIFAR10/100-LT, and ImageNet-Extra provided in [39] when ID is ImageNet-LT.

OOD datasets ($\mathcal{D}_{\mathrm{out}}^{\mathrm{test}}$): For the OOD test data we use six datasets—Texture [5], SVHN [30], LSUN [46], Places365 [49], CIFAR, and TinyImagenet [23]— provided in the SC-OOD benchmark [43] when ID is CIFAR10/100-LT. ImageNet-1k-OOD¹ was used as $\mathcal{D}_{\mathrm{out}}^{\mathrm{test}}$ when ID is ImageNet-LT following [27, 39, 42].

Evaluation metrics: We use six different metrics following existing methods [3, 39, 42] to compare the effectiveness of our model: (1) FPR95 measures the false positive rate of OOD samples when the true positive rate of ID samples is 95%; (2) AUROC is the area under the receiver operating characteristic curve; and (3) AUPR is the area under the precision-recall curve. To measure the ID classification performance we use: (4) ACC as the accuracy on the entire ID test set; (5) ACC_{head} represents the accuracy of the first 50% of the most redundant ID classes; and (6) ACC_{tail}, the accuracy of the rest of the classes.

¹https://github.com/amazon-science/long-tailed-ood-detection

Table 1. OOD detection results for CIFAR10-LT as ID. The best results are shown in bold. Mean over six random runs are reported.

$\mathcal{D}_{ ext{out}}^{ ext{test}}$	Method	AUROC	AUPR	FPR95
	OE	92.59	83.32	25.10
Ħ	PASCL	93.16	84.80	23.26
Texture	BE-OE	95.69	92.38	21.26
	EAT	95.44	92.28	21.50
	Ours	99.50	98.92	1.10
	OE	95.10	97.14	16.15
SVHN	PASCL	96.63	98.06	12.18
⋝	BE-OE	97.74	98.89	9.87
S	EAT	97.92	99.06	9.87
	Ours	99.68	99.71	0.67
	OE	83.40	80.93	56.96
<u> </u>	PASCL	84.43	82.99	57.27
Ŋ.	BE-OE	85.20	84.98	57.95
CIFAR100	EAT	85.93	86.10	54.13
0	Ours	92.08	92.21	35.28
et	OE	86.14	79.33	47.78
Tiny- ImageNet	PASCL	87.14	81.54	47.69
ag a	BE-OE	88.92	84.98	42.38
, T	EAT	89.11	85.43	41.75
	Ours	95.61	93.64	19.93
	OE	91.35	87.62	27.86
5	PASCL	93.17	91.76	26.40
LSUN	BE-OE	94.48	93.15	23.88
_	EAT	95.13	94.12	19.72
	Ours	99.57	99.43	0.74
55	OE	90.07	95.15	34.04
s3(PASCL	91.43	96.28	33.40
8	BE-OE	93.35	97.23	28.25
Places365	EAT	93.68	97.42	26.03
_	Ours	98.12	99.12	5.89
<u>.</u>	OE	89.77	87.25	34.65
	PASCL	90.99	89.24	33.36
Average	BE-OE	92.56	91.94	30.60
Ą	EAT	92.87	92.40	28.83
	Ours	97.43	97.17	10.60

Pre-trained models: As the backbone pre-trained model f, we use the same model architectures used in [3,39,42] for fair comparisons. For experiments on CIFAR10/100-LT, we use the ResNet18 [11] model pre-trained using 32×32 resolution Downsampled ImageNet [4] dataset following [13]. For experiments on ImageNet-LT, the self supervised pre-training model DINO [2] with ResNet50 [11] architecture is used. We carefully select these models to ensure there is no data leakage between the model weights and the data from \mathcal{D}_{in} or \mathcal{D}_{out} .

Graph models: A 3-layer GCN with 512-dimensional hidden features is used as g when ID is CIFAR10/100-LT. For ImageNet-LT, the hidden dimension is increased to 2048.

Baseline methods: We compare our method with SOTA OOD detection methods in LTR: PASCL [39], Balanced EnergyOE (BE-OE) [3], OS [41], COCL [27] and EAT [42]. Three other popular OOD detection methods — OE [15], EnergyOE [25], and OECC [32] — are also compared. For methods using pre-training for OOD detection, we include Pre-train+MSP [13] and Pre-train+Mahalan. [7]. These methods employ the same pre-trained models utilized in our experiments, which are subsequently fine-tuned on training data. We also compare the results with KNN [36], which also finds k-nearest neighbours for OOD detection, but does not utilize graph representation learning unlike in our method. For a fair comparison, we incorporate a fine-

Table 2. OOD detection results for CIFAR100-LT as ID. The best results are shown in bold. Mean over six random runs are reported.

$\mathcal{D}_{ ext{out}}^{ ext{test}}$	Method	AUROC	AUPR	FPR95
	OE	76.71	58.79	68.28
Texture	PASCL	76.01	58.12	67.43
eX.	BE-OE	82.10	73.09	64.19
Ţ	EAT	80.27	71.76	67.53
	Ours	90.88	84.10	39.32
	OE	77.61	86.82	58.04
SVHN	PASCL	80.19	88.49	53.45
5	BE-OE	88.66	92.88	33.79
S	EAT	83.11	89.71	47.78
	Ours	97.02	98.19	10.19
01	OE	62.23	57.57	80.64
CIFAR 10	PASCL	62.33	57.14	79.55
Æ	BE-OE	59.40	54.97	85.16
C	EAT	61.62	55.30	77.97
_	Ours	75.08	74.17	70.62
et	OE	68.04	51.66	76.66
Tiny- ImageNet	PASCL	68.20	51.53	76.11
l'in ag	BE-OE	71.42	56.52	74.22
, E	EAT	68.34	52.79	74.89
	Ours	80.06	68.96	63.48
	OE	77.10	61.42	63.98
rsun	PASCL	77.19	61.27	63.31
S	BE-OE	83.83	71.23	52.04
_	EAT	81.09	67.46	55.02
	Ours	83.29	75.09	59.57
55	OE	75.80	86.68	65.72
Places365	PASCL	76.02	86.52	64.81
<u>3</u>	BE-OE	81.10	89.94	57.52
Б	EAT	78.28	88.20	60.85
	Ours	84.22	92.63	58.87
<u>.</u>	OE	72.91	67.16	68.89
Average	PASCL	73.32	67.18	67.44
ve.	BE-OE	77.75	73.10	61.15
Æ	EAT	75.45	70.87	64.01
	Ours	85.09	82.19	50.34

tuned pre-trained model to apply the *k*-NN distance (Pre-train+KNN). All these methods use auxiliary OOD data for a optimum performance and the same model architectures for fair comparisons. More details on hyper-parameter tuning can be found in the supplementary material.

4.2. Results analysis

OOD detection evaluation results for CIFAR10-LT and CIFAR100-LT as IDs on individual $\mathcal{D}_{\mathrm{out}}^{\mathrm{test}}$ datasets, are summarized in Tab. 1 and Tab. 2, respectively. Overall results for both OOD detection and ID classification with additional baselines for all three ID datasets are summarized in Tab. 3. For CIFAR10-LT and CIFAR100-LT, average values on all six datasets in the SC-OOD benchmark are reported.

The outcomes of our study reveal a noteworthy superiority of our approach over other baseline methods in both OOD detection and ID classification across all ID datasets. Notably, in the more demanding CIFAR100-LT scenario, our method exhibits substantial improvements, having enhanced average values of 6.05% for AUROC, 8.19% for AUPR, 8.51% for FPR95, and 6.95% for ACC, respectively, compared to the second best method.

In the context of large-scale ImageNet-LT, which involves a broader spectrum of IDs, similar improvements of 2.49% for AUROC and 1.53% for AUPR are observed. The discernible trend in our findings indicates a pronounced en-

Table 3. OOD detection results and ID classification results for CIFAR10-LT, CIFAR100-LT and ImageNet-LT as ID, with additional baselines. For CIFAR10-LT and CIFAR100-LT average values on all six $\mathcal{D}_{\mathrm{out}}^{\mathrm{test}}$ are reported. The best and second-best results are bolded and underlined, respectively. Mean over six random runs are reported.

$\mathcal{D}_{\mathrm{in}}$	$\mathcal{D}_{ ext{out}}^{ ext{test}}$	Method	AUROC	AUPR	FPR95	ACC	ACChead	ACC _{tail}
		OECC	87.28	86.29	45.24	61.24	84.96	37.52
		EnergyOE	91.92	91.97	33.79	74.25	87.74	60.76
H		OE	89.77	87.25	34.65	73.86	84.92	62.80
1-0		OS	91.94	89.35	36.92	75.61	84.32	66.90
<u>R</u>	SC-OOD	PASCL	90.99	89.24	33.36	77.07	86.12	68.02
CIFAR10-LT		BE-OE	92.56	91.94	30.60	81.32	85.14	77.50
ひ		EAT	92.87	92.40	28.83	81.42	85.94	76.90
		COCL	93.28	92.89	30.88	81.56	85.22	77.90
		Pre-train+KNN	90.20	89.59	55.53	85.66	93.20	<u>78.12</u>
		Pre-train+MSP	94.10	92.91	23.15	85.66	93.20	78.12
		Pre-train+Mahalan.	92.89	93.01	28.79	85.66	93.20	<u>78.12</u>
		Ours	97.43	97.17	10.60	89.74	90.71	88.76
		OECC	70.38	66.87	73.15	32.93	52.31	13.02
		EnergyOE	76.40	72.24	64.54	40.63	63.30	17.96
Ľ		OE	72.91	67.16	68.89	39.51	60.98	18.04
CIFAR 100-LT		OS	74.37	70.42	78.18	40.92	58.49	23.34
R10	SC-OOD	PASCL	73.32	67.18	67.44	43.09	59.50	26.68
₹		BE-OE	77.75	73.10	61.15	45.72	56.72	34.72
CI		EAT	75.45	70.87	64.01	45.31	62.76	27.86
		COCL	78.25	73.58	74.09	46.41	63.38	29.44
		Pre-train+KNN	72.57	67.28	77.03	56.02	<u>73.82</u>	<u>38.22</u>
		Pre-train+MSP	79.04	74.00	58.85	56.02	73.82	38.22
		Pre-train+Mahalan.	74.91	72.38	67.30	56.02	73.82	<u>38.22</u>
		Ours	85.09	82.19	50.34	62.97	74.76	51.17
		OECC	63.07	63.05	86.90	38.25	54.45	22.71
		EnergyOE	65.33	67.40	88.22	43.27	62.81	23.72
\Box		OE	66.33	68.29	88.22	37.60	54.29	20.90
급	ImageNet-	OS	68.01	69.53	88.97	45.23	56.25	34.21
e <mark>S</mark>	1k-OOD	PASCL	68.00	70.15	87.53	45.49	54.73	36.26
ImageNet-LT	IK-OOD	BE-OE	66.89	68.81	87.70	47.81	58.31	<u>37.32</u>
<u> </u>		EAT	69.84	69.25	87.63	46.79	59.46	34.12
		COCL	69.93	69.78	87.46	<u>51.11</u>	74.17	28.05
		Pre-train+KNN	70.65	70.42	78.14	48.79	68.02	29.56
		Pre-train+MSP	72.27	74.46	85.09	48.79	68.02	29.56
		Pre-train+Mahalan.	68.91	69.84	85.91	48.79	68.02	29.56
		Ours	74.76	75.99	82.42	51.57	64.84	38.31

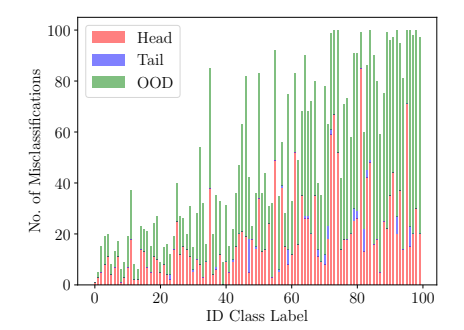
Table 4. Ablation study. Average values on all six \mathcal{D}_{out}^{test} are reported. The best and second-best results are bolded and underlined, respectively. Mean over six random runs are reported.

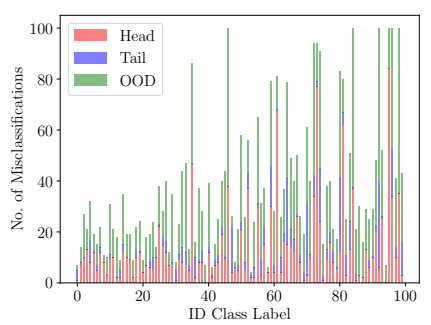
$\mathcal{D}_{ ext{in}}$	Pre-train	Gau.	GRL	Method	AUROC	AUPR	FPR95	ACC	ACC _{head}	ACC _{tail}
r .	Х	Х	Х	Scratch (OE)	89.77	87.25	34.65	73.86	84.92	62.80
Ş	X	X	✓	Scratch+GCN	84.25	79.20	39.22	66.73	76.84	56.62
10	✓	X	X	Pre-train	91.37	91.29	36.36	76.34	92.92	59.76
ΑR	✓	X	1	Pre-train+GCN	96.33	95.89	14.28	86.69	90.15	83.22
CIFAR10-LT	✓	1	X	Pre-train+Gau.	92.59	93.15	34.06	80.23	94.18	66.28
0	✓	1	1	Pre-train+Gau.+GCN(ours)	97.43	97.17	10.60	89.74	90.71	88.76
	Х	Х	Х	Scratch (OE)	72.91	67.16	68.89	39.51	60.98	18.04
R100-LT	X	X	✓	Scratch+GCN	73.93	65.97	68.58	40.74	57.66	23.82
100	✓	X	Х	Pre-train	72.17	68.43	71.23	50.38	74.92	25.84
^K R	✓	X	✓	Pre-train+GCN	81.40	78.05	58.88	54.48	69.45	39.51
CIFA	✓	1	Х	Pre-train+Gau.	78.01	74.64	64.11	55.66	77.94	33.38
	✓	1	1	Pre-train+Gau.+GCN(ours)	85.09	82.19	50.34	62.97	74.76	51.17

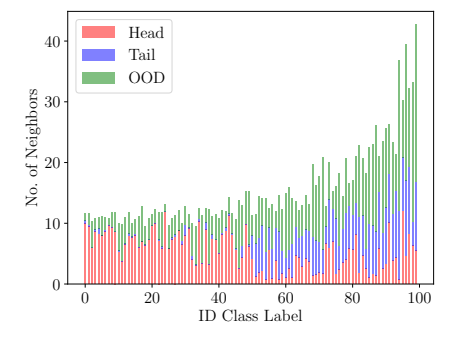
hancement in overall ID classification accuracy, particularly in the tail-classes. This is evidenced by the 10.64% improvement in CIFAR10-LT, 12.95% in CIFAR100-LT, and 1% in ImageNet-LT, underscoring the substantial benefits our method brings to the tail-classes.

4.3. Ablation study

Importance of different components: We present the results of ablation studies on each of the three key components outlined in our methodology in Sec. 3: (i) graph repre-







- (a) Misclassification Distribution Baseline.
- (b) Misclassification Distribution Ours.
- (c) Neighbor Node Distribution.

Figure 3. Distribution of number of ID misclassifications over each class for CIFAR100-LT, with (a) one of the baselines "Pre-train" and (b) our method. (c) Head-class ID, tail-class ID and OOD neighbor node distribution over each ID class of CIFAR100-LT. Average neighbor values per each class are plotted due to the long-tailed nature. ID class labels higher than 50 belong to tail-classes.

sentation learning (indicated as GRL), (ii) selection of pretrained embeddings, and (iii) Gaussianization of pre-trained activation layers (indicated as Gau.).

To verify the performance gain from pre-training, we substitute the pre-trained backbone model with a baseline ResNet18 trained from scratch using OE [15] to extract the initial features needed for the input graph. The results (denoted as Scratch+GCN in Tab. 4) indicate a notable decrease compared to the results achieved with the Pre-train+GCN combination. Also, applying Gaussianization to pre-trained activation layers (Pre-train+Gau.+GCN) further improves the performance by a large margin compared to Pre-train+GCN alone. Furthermore, note that applying GRL on top of a backbone trained from scratch barely brings an improvement compared to a linear classifier on the same backbone (Scratch+GCN vs. Scratch). This indicates the importance of selecting the initial feature representations of the graph for GRL to be successful.

Importance of graph structure: To shed light on the importance of leveraging inter-sample relationships within the data, we also look at the distribution of misclassifications for CIFAR100-LT. As shown in Fig. 3a, the performance of the baseline model in the long-tailed setting gets worse as we move towards rare classes. Interestingly, the OOD misses are also substantially higher for the tail classes. These observations demonstrate the need for a better feature representation to simultaneously (i) distinguish the tail classes from the head, and (ii) separate the tail from the OOD data. Our graph structure is designed to facilitate this.

In Fig. 3c we also plot the neighbor node distribution of input graph obtained by averaging the number of tail, head, and OOD neighbors for each ID node within a class. As can be seen in this figure, the proposed graph structure creates a clear distinction between the head and tail nodes. In particular, we see that most of the neighbors for the tail classes are also tail class. Additionally, most OOD samples are assigned to a neighborhood of tail samples where there is more ambiguity that needs to be assessed. The successful

performance of our method, as shown in Fig. 3b, demonstrates that adding an inductive bias leveraging the intersample information between data points can help us protect the tail classes and have a more balanced error distribution.

More ablation studies on model architecture, graph structure, pre-training dataset, computational cost, and sensitivity analysis on key hyper-parameters can be found in the supplementary material.

5. Discussion and conclusion

Developing models robust to OOD samples in the presence of long-tailed IDs is important and challenging at the same time. Specifically, it is vital to maintain accuracy for tail-class categories while ensuring robustness to OOD samples, particularly in certain applications. For instance, consider the task of automated skin cancer detection. It is essential to distinguish between known rare skin lesion categories and unknown lesions effectively.

In this paper, we proposed a graph-based solution to address this problem on vision datasets. To this end, we used the k-NN graph built over an appropriate initial representation. By leveraging the feature space of a pre-trained model, which is adjusted using the process of Gaussianization, our graph structure can fully exploit the complex interrelationships within the data. We further refined our initial graph structure using GCNs to arrive at a feature space suitable for our intended downstream task. Through extensive experiments on both OOD detection and ID classification, we demonstrate the effectiveness of our method establishing a new SOTA.

Acknowledgments. This research was undertaken using the LIEF HPC-GPGPU Facility hosted at the University of Melbourne. This Facility was established with the assistance of LIEF Grant LE170100200. Sarah Erfani is in part supported by Australian Research Council (ARC) Discovery Early Career Researcher Award (DECRA) DE220100680.

References

- Kaidi Cao, Colin Wei, Adrien Gaidon, Nikos Arechiga, and Tengyu Ma. Learning imbalanced datasets with labeldistribution-aware margin loss. In *NeurIPS*, 2019.
- [2] Mathilde Caron, Hugo Touvron, Ishan Misra, Hervé Jégou, Julien Mairal, Piotr Bojanowski, and Armand Joulin. Emerging properties in self-supervised vision transformers. In *ICCV*, 2021. 6
- [3] Hyunjun Choi, Hawook Jeong, and Jin Young Choi. Balanced energy regularization loss for out-of-distribution detection. In CVPR, pages 15691–15700, 2023. 1, 3, 4, 5, 6
- [4] Patryk Chrabaszcz, Ilya Loshchilov, and Frank Hutter. A downsampled variant of imagenet as an alternative to the CI-FAR datasets. *CoRR*, abs/1707.08819, 2017. 6
- [5] Mircea Cimpoi, Subhransu Maji, Iasonas Kokkinos, Sammy Mohamed, and Andrea Vedaldi. Describing textures in the wild. In CVPR, pages 3606–3613, 2014. 5
- [6] Uno Fang, Jianxin Li, Xuequan Lu, Ajmal Mian, and Zhaoquan Gu. Robust image clustering via context-aware contrastive graph learning. *PR*, 138:109340, 2023. 3
- [7] Stanislav Fort, Jie Ren, and Balaji Lakshminarayanan. Exploring the limits of out-of-distribution detection. In *NeurIPS*, pages 7068–7081, 2021. 1, 3, 6
- [8] Justin Gilmer, Samuel S Schoenholz, Patrick F Riley, Oriol Vinyals, and George E Dahl. Neural message passing for quantum chemistry. In *ICML*, pages 1263–1272, 2017. 3
- [9] Sorin Grigorescu, Bogdan Trasnea, Tiberiu Cocias, and Gigel Macesanu. A survey of deep learning techniques for autonomous driving. *Journal of Field Robotics*, 37(3):362– 386, 2020. 1
- [10] Will Hamilton, Zhitao Ying, and Jure Leskovec. Inductive representation learning on large graphs. In *NeurIPS*, volume 30, 2017. 3, 5
- [11] Kaiming He, Xiangyu Zhang, Shaoqing Ren, and Jian Sun. Deep residual learning for image recognition. In CVPR, pages 770–778, 2016. 6
- [12] Dan Hendrycks and Kevin Gimpel. A baseline for detecting misclassified and out-of-distribution examples in neural networks. In *ICLR*, 2017. 1, 2, 4
- [13] Dan Hendrycks, Kimin Lee, and Mantas Mazeika. Using pre-training can improve model robustness and uncertainty. In *ICML*, pages 2712–2721, 2019. 1, 3, 6
- [14] Dan Hendrycks, Xiaoyuan Liu, Eric Wallace, Adam Dziedzic, Rishabh Krishnan, and Dawn Song. Pretrained transformers improve out-of-distribution robustness. In Dan Jurafsky, Joyce Chai, Natalie Schluter, and Joel R. Tetreault, editors, *ACL*, pages 2744–2751, 2020. 1, 3
- [15] Dan Hendrycks, Mantas Mazeika, and Thomas G. Dietterich. Deep anomaly detection with outlier exposure. In *ICLR*, 2019. 1, 2, 3, 4, 6, 8
- [16] Dan Hendrycks, Mantas Mazeika, Saurav Kadavath, and Dawn Song. Using self-supervised learning can improve model robustness and uncertainty. In *NeurIPS*, 2019. 3
- [17] Sergey Ioffe. Batch normalization: Accelerating deep network training by reducing internal covariate shift. In *ICML*, 2015. 4

- [18] Sergey Ioffe and Christian Szegedy. Batch normalization: Accelerating deep network training by reducing internal covariate shift. In *ICML*, pages 448–456, 2015. 2, 5
- [19] Taejong Joo, Donggu Kang, and Byunghoon Kim. Regularizing activations in neural networks via distribution matching with the wasserstein metric. In *ICLR*, 2020. 2, 5, 4
- [20] Abhishek Joshi, Sathish Chalasani, and Kiran Nanjunda Iyer. Semantic driven energy based out-of-distribution detection. In *IJCNN*, pages 01–08. IEEE, 2022. 3
- [21] Thomas N. Kipf and Max Welling. Semi-supervised classification with graph convolutional networks. In *ICLR*, 2017. 3, 4, 5
- [22] Alex Krizhevsky and Geoffrey Hinton. Learning multiple layers of features from tiny images. Technical report, University of Toronto, Toronto, Ontario, 2009. 5
- [23] Ya Le and Xuan Yang. Tiny imagenet visual recognition challenge. CS 231N, 7(7):3, 2015. 5
- [24] Kimin Lee, Kibok Lee, Honglak Lee, and Jinwoo Shin. A simple unified framework for detecting out-of-distribution samples and adversarial attacks. In *NeurIPS*, 2018. 1, 2
- [25] Weitang Liu, Xiaoyun Wang, John Owens, and Yixuan Li. Energy-based out-of-distribution detection. In *NeurIPS*, pages 21464–21475, 2020. 1, 3, 6
- [26] Ziwei Liu, Zhongqi Miao, Xiaohang Zhan, Jiayun Wang, Boqing Gong, and Stella X Yu. Large-scale long-tailed recognition in an open world. In CVPR, pages 2537–2546, 2019. 5
- [27] Wenjun Miao, Guansong Pang, Xiao Bai, Tianqi Li, and Jin Zheng. Out-of-distribution detection in long-tailed recognition with calibrated outlier class learning. In AAAI, volume 38, pages 4216–4224, 2024. 1, 3, 5, 6
- [28] Aashish Kumar Misraa, Ajinkya Kale, Pranav Aggarwal, and Ali Aminian. Multi-modal retrieval using graph neural networks. CoRR, abs/2010.01666, 2020. 3
- [29] Sina Mohseni, Mandar Pitale, JBS Yadawa, and Zhangyang Wang. Self-supervised learning for generalizable out-ofdistribution detection. In AAAI, volume 34, pages 5216– 5223, 2020. 3
- [30] Yuval Netzer, Tao Wang, Adam Coates, Alessandro Bissacco, Bo Wu, and Andrew Y Ng. Reading digits in natural images with unsupervised feature learning. In *Proceedings of the NeurIPS Workshop on Deep Learning and Unsupervised Feature Learning*, 2011. 5
- [31] Anh Nguyen, Jason Yosinski, and Jeff Clune. Deep neural networks are easily fooled: High confidence predictions for unrecognizable images. In *CVPR*, pages 427–436, 2015. 1
- [32] Aristotelis-Angelos Papadopoulos, Mohammad Reza Rajati, Nazim Shaikh, and Jiamian Wang. Outlier exposure with confidence control for out-of-distribution detection. *Neuro-computing*, 441:138–150, 2021. 3, 6
- [33] Olga Russakovsky, Jia Deng, Hao Su, Jonathan Krause, Sanjeev Satheesh, Sean Ma, Zhiheng Huang, Andrej Karpathy, Aditya Khosla, Michael Bernstein, et al. Imagenet large scale visual recognition challenge. *IJCV*, 115:211–252, 2015. 3, 5, 1
- [34] Chandramouli Shama Sastry and Sageev Oore. Detecting out-of-distribution examples with gram matrices. In *ICML*, pages 8491–8501, 2020. 2

- [35] Jenny Denise Seidenschwarz, Ismail Elezi, and Laura Leal-Taixé. Learning intra-batch connections for deep metric learning. In *ICML*, pages 9410–9421, 2021. 4
- [36] Yiyou Sun, Yifei Ming, Xiaojin Zhu, and Yixuan Li. Out-ofdistribution detection with deep nearest neighbors. In *ICML*, pages 20827–20840. PMLR, 2022. 1, 2, 6
- [37] Antonio Torralba, Rob Fergus, and William T Freeman. 80 million tiny images: A large data set for nonparametric object and scene recognition. *IEEE TPAMI*, 30(11):1958–1970, 2008. 5
- [38] Vivek Trivedy and Longin Jan Latecki. Cnn2graph: Building graphs for image classification. In CWCV, 2023. 3
- [39] Haotao Wang, Aston Zhang, Yi Zhu, Shuai Zheng, Mu Li, Alex J Smola, and Zhangyang Wang. Partial and asymmetric contrastive learning for out-of-distribution detection in long-tailed recognition. In *ICML*, pages 23446–23458, 2022. 1, 3, 4, 5, 6
- [40] Zhongdao Wang, Liang Zheng, Yali Li, and Shengjin Wang. Linkage based face clustering via graph convolution network. In CVPR, pages 1117–1125, 2019. 3
- [41] Hongxin Wei, Lue Tao, Renchunzi Xie, Lei Feng, and Bo An. Open-sampling: Exploring out-of-distribution data for re-balancing long-tailed datasets. In *ICML*, pages 23615– 23630. PMLR, 2022. 3, 6
- [42] Tong Wei, Bo-Lin Wang, and Min-Ling Zhang. Eat: Towards long-tailed out-of-distribution detection. In *AAAI*, volume 38, pages 15787–15795, 2024. 1, 3, 5, 6
- [43] Jingkang Yang, Haoqi Wang, Litong Feng, Xiaopeng Yan, Huabin Zheng, Wayne Zhang, and Ziwei Liu. Semantically coherent out-of-distribution detection. In *ICCV*, pages 8301– 8309, 2021. 5
- [44] Lei Yang, Xiaohang Zhan, Dapeng Chen, Junjie Yan, Chen Change Loy, and Dahua Lin. Learning to cluster faces on an affinity graph. In *CVPR*, pages 2298–2306, 2019. 3
- [45] Sijie Yang, Fei Zhu, Xinghong Ling, Quan Liu, and Peiyao Zhao. Intelligent health care: Applications of deep learning in computational medicine. Frontiers in Genetics, 12:607471, 2021.
- [46] Fisher Yu, Yinda Zhang, Shuran Song, Ari Seff, and Jianxiong Xiao. LSUN: construction of a large-scale image dataset using deep learning with humans in the loop. *CoRR*, abs/1506.03365, 2015. 5
- [47] Matthew D Zeiler and Rob Fergus. Visualizing and understanding convolutional networks. In ECCV, pages 818–833, 2014. 3, 5
- [48] Yaobin Zhang, Weihong Deng, Mei Wang, Jiani Hu, Xian Li, Dongyue Zhao, and Dongchao Wen. Global-local gcn: Large-scale label noise cleansing for face recognition. In CVPR, pages 7731–7740, 2020. 3
- [49] Bolei Zhou, Agata Lapedriza, Aditya Khosla, Aude Oliva, and Antonio Torralba. Places: A 10 million image database for scene recognition. *IEEE TPAMI*, 40(6):1452–1464, 2017.

Exploiting Inter-Sample Information for Long-tailed Out-of-Distribution Detection

Supplementary Material

A. Hyper-parameter tuning

We used a validation set of 10% and 17% of training data for CIFAR10/100-LT and ImageNet-LT respectively. For experiments on CIFAR10/100-LT, we empirically set k = 7 to create the k-NN graphs with self-loops using 512-dimensional pre-trained embeddings. The pre-trained model is trained for 100 epochs using SGD with Nesterov momentum and a cosine learning rate, with batch size 256 following [13]. To update the BN statistics, BN layers are fine-tuned for another 20 epochs with a learning rate of 0.001 using all the training data. GCN is trained for 200 epochs using the Adam optimizer with an initial learning rate of 0.001 and a cosine annealing learning rate scheduler. For ImageNet-LT, k is set to 2 and pre-trained embeddings are 2048-dimensional. BN layers are fine-tuned for 20 epochs with a learning rate of 0.001. GCN is trained for 250 epochs using the Adam optimizer with an initial learning rate of 0.01 which is decayed by a factor of 10 at epoch 15 and 100. On all datasets, we set $\lambda = 0.5$ following [39].

B. Additional ablation studies

B.1. Sensitivity analysis on k and λ

As seen, given a meaningful feature space, our graph combination can achieve a remarkable improvement, especially in terms of FPR95 and ACCtail. However, the improvement in tail-classes compensates for a slight decline in ACC_{head}. This compensation can be attributed to the interplay between samples from tail-classes and the representative samples from head-classes. To provide a better explanation, we observe the behaviour of head and tail classes concerning the number of neighbor connections available for each sample. By increasing the k in the k-NN graph, we increase the number of edges in the overall graph. As we can see in Fig. 4, the increase in k causes ACC_{head} to drop, while ACC_{tail} continues to grow along with the overall ACC. This suggests that too much neighborhood information around head-samples is undesirable, leading to oversmoothing of representative samples. In contrast, this additional information benefits the tail-samples, resulting in a much-improved ACC_{tail} and a higher overall ACC.

We also conduct an ablation study on λ that controls the importance of the OE loss term as summarized in Tab. 5. The performance of our method is stable with respect to

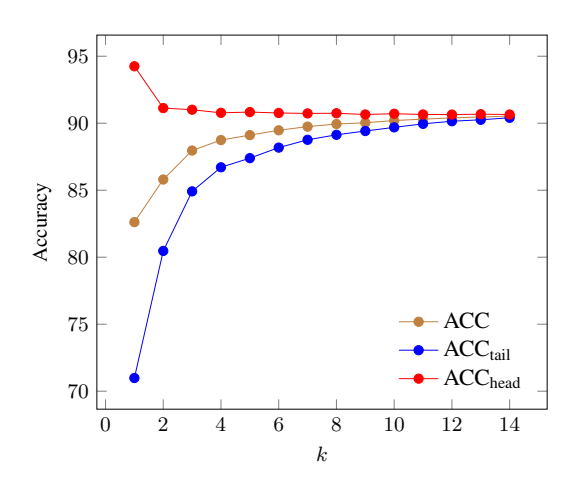


Figure 4. Variation of CIFAR10-LT ID classification accuracy over selection of k in the k-NN graph.

Table 5. Ablation study on λ for CIFAR10-LT as ID. Average values on all six $\mathcal{D}_{\mathrm{out}}^{\mathrm{test}}$ are reported.

$\overline{\lambda}$	AUROC	AUPR	FPR95	ACC	ACChead	ACC _{tail}
0.00	96.95	96.58	12.10	89.77	90.84	88.70
0.25		97.03	10.70	89.77	90.78	88.76
0.50						88.73
1.00	97.46	97.22	10.70	89.64	90.70	88.58

different λ values, showing a notable decrease only when λ is set to 0.

B.2. Model architecture

In Tab. 3, we employ ResNet18 as the pre-trained backbone model, aligning with prior work [3, 39] that addresses OOD detection in long-tailed recognition. In this section, we demonstrate the versatility of our method across various model architectures. Specifically, Fort *et al.* [7] suggested that utilizing a pre-trained ViT can enhance OOD detection, although they did not evaluate their method on long-tailed IDs. We therefore replace pre-trained ResNet18 model with a ViT-L_16 model pre-trained on ImageNet-1k [33] dataset. We observed that for ViTs, it would be more helpful to fine-tune the entire network before feature extraction. This results in even better performance (ViT-L_16+GCN in Tab. 6) than the ResNet18 (ResNet18+GCN) underscoring the effectiveness of our method across diverse model architectures.

Table 6. Ablation study on model architecture for CIFAR10-LT and CIFAR100-LT as ID. Average values on all six $\mathcal{D}_{\mathrm{out}}^{\mathrm{test}}$ are reported. The best results are shown in bold. Mean over six random runs are reported.

$\mathcal{D}_{\mathrm{in}}$	Method	AUROC	AUPR	FPR95	ACC	ACC _{head}	ACC _{tail}
	ResNet18	92.59	93.15	34.06	80.23	94.18	66.28
CIFAR10-LT	ResNet18+GCN	97.43	97.17	10.60	89.74	90.71	88.76
CITAK10-LI	ViT-L_16	97.81	96.55	7.66	94.97	97.30	92.64
	ViT-L_16+GCN	98.34	97.10	4.36	95.80	96.18	95.42
	ResNet18	78.01	74.64	64.11	55.66	77.94	33.38
CIFAR100-LT	ResNet18+GCN	85.09	82.19	50.34	62.97	74.76	51.17
CIFAK100-LI	ViT-L_16	86.81	77.51	37.51	69.74	88.62	50.86
	ViT-L_16+GCN	89.26	79.33	28.31	74.90	86.20	63.61

Table 7. Ablation study on batch-wise inference for CIFAR10-LT as ID. Average values on all six $\mathcal{D}_{\mathrm{out}}^{\mathrm{test}}$ are reported. The best results are shown in bold. Mean over six random runs are reported.

Batch Size	AUROC	AUPR	FPR95	ACC	ACChead	ACC _{tail}
512	95.96	95.84	16.43	83.19	87.87	78.50
1024	96.57	96.41	14.13	86.35	88.81	83.90
2048	96.86	96.66	13.01	87.58	89.37	85.80
4096	97.11	96.90	11.98	88.63	90.14	87.11
8192	97.25	96.97	11.29	89.15	90.40	87.90
All Samples	97.43	97.17	10.60	89.74	90.71	88.76

Table 8. Ablation study on batch-wise inference for CIFAR100-LT as ID. Average values on all six $\mathcal{D}_{\mathrm{out}}^{\mathrm{test}}$ are reported. The best results are shown in bold. Mean over six random runs are reported.

Batch Size	AUROC	AUPR	FPR95	ACC	ACC _{head}	ACCtail
512	69.15	67.49	77.66	32.90	48.13	17.68
1024	75.22	73.56	69.90	42.17	57.75	26.59
2048	79.81	77.79	62.14	50.45	65.33	35.56
4096	82.51	80.08	56.43	56.09	69.73	42.46
8192	83.84	81.21	53.30	59.42	71.94	46.90
All Samples	85.09	82.19	50.34	62.97	74.76	51.17

OOD

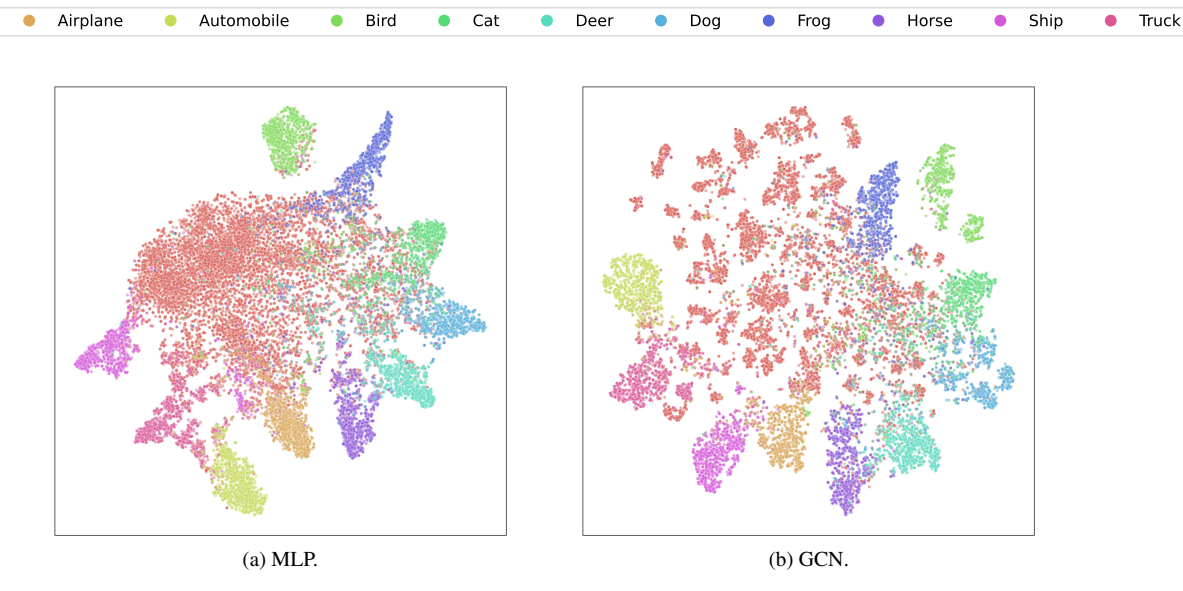


Figure 5. Feature space representations obtained from the (a) MLP and (b) GCN models for CIFAR10-LT as ID test set and CIFAR-100 as OOD test set using t-SNE. Equal number of test samples from each ID class are visualized. The GCN demonstrates distinct gaps between the decision boundaries of ID and OOD samples compared to the MLP.

Table 9. Performance on CIFAR10-LT with all CIFAR10-related classes removed from the pre-training dataset. Average values on all six $\mathcal{D}_{\mathrm{out}}^{\mathrm{test}}$ are reported.

Method						
cifar_excluded	96.55	96.33	14.66	87.78	88.95	86.60
All	97.43	97.17	10.60	89.74	90.71	88.76

B.3. An alternative inference method

In our method, during inference, we construct a test graph using all ID and OOD test samples. However, in practical scenarios, inference is typically performed on batches of test samples which may belong to either ID or OOD. To ensure compatibility with such practical scenarios, we conduct experiments by processing batches of test samples instead of the full test data. In particular, for each randomly selected batch of data, we generate the *k*-NN graph over these data points alone to make the inference on that specific batch. Results for CIFAR10-LT and CIFAR100-LT as ID are indicated in Tab. 7 and Tab. 8, respectively. Results indicate that our method exhibits stability in batch inference, delivering nearly comparable performance to processing all samples, particularly noticeable with larger batch sizes.

B.4. Effect of the pre-training dataset

To further examine the effect of the pre-training dataset, similar to an ablation study of [13], we removed 153 CIFAR-10 related classes from Downsampled ImageNet and reran the experiments for CIFAR10-LT. This further ensures the pre-trained model has not seen any tail-class or super-class related instances. Results shown in Tab. 9 indicate similar performance gains. As we can see, our method still achieves SOTA (w.r.t. other baselines in Tab. 3) with only a small degradation compared to the model that uses all samples. This demonstrates that the pre-trained model do not rely on seeing CIFAR-10 related samples, and that simply training on more natural images increases the overall performance [13].

B.5. Graph structure

To further validate the importance of the graph structure, we replace the shallow linear classifier in the "Pretrain+Gau." baseline with a deeper Multi-Layer Perceptron (MLP) classifier. This MLP has an equivalent number of layers and trainable parameters as the GCN. Results for CIFAR10-LT and CIFAR100-LT as ID are shown in Tab. 10 and Tab. 11, respectively. As the MLP does not consider any inter-sample relationships, the outcome demonstrates lower performance for the "Pre-train+Gau.+MLP" baseline compared to the combination with GCN (Pretrain+Gau.+GCN). This observation is particularly evident in terms of FPR95 and ACC_{tail}.

Table 10. Ablation study on importance of GRL using a MLP for CIFAR10-LT as ID. The best results are shown in bold. Mean over six random runs are reported.

(a) OOD detection results.

$\mathcal{D}_{ ext{out}}^{ ext{test}}$	Method	AUROC	AUPR	FPR95
Texture	Pre-train+Gau.+MLP	99.12	98.54	3.21
Texture	Pre-train+Gau.+GCN	99.50	98.92	1.10
SVHN	Pre-train+Gau.+MLP	99.35	99.73	2.61
SVIIIV	Pre-train+Gau.+GCN	99.68	99.71	0.67
CIFAR100	Pre-train+Gau.+MLP	91.11	91.70	41.16
CITAKIOO	Pre-train+Gau.+GCN	92.08	92.21	35.28
TinyImageNet	Pre-train+Gau.+MLP	94.40	92.93	28.66
Tillylillagervet	Pre-train+Gau.+GCN	95.61	93.64	19.93
LSUN	Pre-train+Gau.+MLP	98.85	98.84	4.87
LSUN	Pre-train+Gau.+GCN	99.57	99.43	0.74
Places365	Pre-train+Gau.+MLP	97.55	99.17	14.86
1 14008303	Pre-train+Gau.+GCN	98.12	99.12	5.89
Average	Pre-train+Gau.+MLP	96.73	96.82	15.90
Average	Pre-train+Gau.+GCN	97.43	97.17	10.60

(b) ID classification results.

Method	ACC	ACChead	ACC _{tail}
Pre-train+Gau.+MLP	87.63	94.64	80.61
Pre-train+Gau.+GCN	89.74	90.71	88.76

Table 11. Ablation study on importance of GRL using a MLP for CIFAR100-LT as ID. The best results are shown in bold. Mean over six random runs are reported.

(a) OOD detection results.

$\mathcal{D}_{\mathrm{out}}^{\mathrm{test}}$	Method	AUROC	AUPR	FPR95
Texture	Pre-train+Gau.+MLP	90.95	84.76	39.54
Texture	Pre-train+Gau.+GCN	90.88	84.10	39.32
SVHN	Pre-train+Gau.+MLP	95.20	97.51	18.89
SVIIN	Pre-train+Gau.+GCN	97.02	98.19	10.19
CIFAR10	Pre-train+Gau.+MLP	73.39	68.21	70.79
CIFAKIO	Pre-train+Gau.+GCN	75.08	74.17	70.62
TinyImageNet	Pre-train+Gau.+MLP	79.19	67.42	65.46
Tillytillageriet	Pre-train+Gau.+GCN	80.06	68.96	63.48
LSUN	Pre-train+Gau.+MLP	81.03	72.32	68.22
LSUN	Pre-train+Gau.+GCN	83.29	75.09	59.57
Places365	Pre-train+Gau.+MLP	83.21	92.05	60.41
1 laces303	Pre-train+Gau.+GCN	84.22	92.63	58.87
A	Pre-train+Gau.+MLP	83.83	80.38	53.88
Average	Pre-train+Gau.+GCN	85.09	82.19	50.34
	(1) TD 1 10 1			

(b) ID classification results.

Method	ACC	ACC _{head}	ACCtail
Pre-train+Gau.+MLP	61.62	79.12	44.13
Pre-train+Gau.+GCN	62.97	74.76	51.17

This fact can be further clarified by examining the feature space representations from these two models, as depicted in Fig. 5. As seen, there are distinct gaps between the decision boundaries of ID and OOD samples in the representations obtained from the GCN (Fig. 5b) compared to the MLP (Fig. 5a).

Table 12. Comparison of the training and inference speed (averaged per-image) for CIFAR100-LT vs. CIFAR10 experiments on an NVIDIA-A100 GPU. For our method, different k values (indicated in brackets) are compared.

Method	Train. time(s)	Infer. time(ms)		
OECC	715.57	0.27		
EnergyOE	687.40	0.24		
OE	690.09	0.11		
PASCL	1265.63	0.13		
BE-OE	706.87	0.24		
EAT	3526.58	0.14		
COCL	659.74	0.11		
Pre-train+KNN	603.96	1.67		
Ours	478.51 (k=3)	2.09 (k=3)		
	533.13 (k=7)	2.10 (k=7)		
	620.10 (k=10)	2.11 (k=10)		

B.6. Computational cost

Tab. 12 compares the training and inference times of our method with other baselines. For our method, the total training time includes the time taken for Gaussianization, graph creation, and GCN training. Despite these components, the overall training time remains shorter because we employed a lightweight GCN model with only 578,860 parameters. This is in contrast to most of the other methods, which require 11,599,752 parameters to be trained from scratch. However, similar to KNN method, inference takes slightly longer than other methods due to the overhead introduced by k nearest neighbour search and the graph creation process. Notably, varying k values does not significantly impact the inference speed.

B.7. Performance on balanced ID datasets

We also compare the performance of our method on balanced ID datasets in Tab. 13. Note that some LTR baselines, including PASCL, OS, EAT, and COCL (which we did not include in the table), cannot be directly evaluated or reduced to other baselines when there are zero tail-classes. For our method, we used the same experimental settings as in the LT experiments, except that the imbalance ratio ρ was set to 1. As shown, our method outperforms most baselines for OOD detection across all metrics while demonstrating comparable performance in ID classification accuracy. There is a small effect of reduction of ID accuracy, when using higher k values, which result in larger number of neighbors around ID nodes in the graph. However, the inter-sample relationships between nodes greatly benefit the OOD detection. This is part of the trade-off between leveraging useful relational information and the risk of over-smoothing, a common issue inherent to many graph-based approaches.

Table 13. OOD detection results and ID classification results for balanced CIFAR-10 and CIFAR-100 as ID. Average values on all six $\mathcal{D}_{\mathrm{out}}^{\mathrm{test}}$ are reported. The best results are bolded. Mean over six random runs are reported.

$\overline{\mathcal{D}_{ ext{in}}}$	Method	AUROC	AUPR	FPR95	ACC
CIFAR-10	OECC	96.33	95.38	14.36	91.57
	EnergyOE	96.77	96.72	14.82	93.30
	OE	96.67	95.97	13.80	93.64
	BE-OE	96.83	96.70	14.51	93.00
	Pre-train+KNN	94.82	94.03	26.36	95.91
	Ours	97.84	97.66	8.86	91.40
CIFAR-100	OECC	84.03	77.94	45.26	69.55
	EnergyOE	85.84	80.99	43.02	74.95
	OE	83.92	78.07	49.49	71.36
	BE-OE	85.85	80.91	42.93	74.83
	Pre-train+KNN	85.52	80.71	55.56	79.82
	Ours	87.17	83.91	43.62	70.37

B.8. Detailed ablation results

In Table 4, we presented an ablation study over various components of our proposed approach. Due to space limitations, we omitted the detailed results over separate OOD data. Detailed ablation study results over separate $\mathcal{D}_{\text{out}}^{\text{test}}$ for CIFAR10-LT and CIFAR100-LT are shown in Tab. 14 and Tab. 15, respectively.

C. More details on Gaussianization

Regularization and normalization techniques are commonly applied to neural networks to ensure stable training and improved generalization performance [17, 19]. Among various normalization methods for controlling hidden activations, Gaussianization ensures that the activation layer representations follow a standard normal distribution. This approach relies on batch normalization (BN) layers, which take hidden activations as input to the next layer and normalize them to have zero mean and unit variance. During inference, the network uses 'running statistics' (running mean- μ_{running} and running variance- σ_{running}) that are computed and updated during training to normalize activations, i.e.,

$$\hat{x}_i = \frac{x_i - \mu_{\text{running}}}{\sqrt{\sigma_{\text{running}}^2 + \epsilon}},$$

where x_i denotes the current data input and ϵ is a small constant added for numerical stability. In our pipeline, we used a backbone model f pre-trained on a different dataset $(\mathcal{D}_{\text{pretrain}})$ to extract initial feature representations for each training input. However, when calculating these feature representations, the running statistics from $\mathcal{D}_{\text{pretrain}}$ are used, which differ from those of the current training data $(\mathcal{D}_{\text{train}})$. This results in a misalignment of the activations from the

intended standard normal distribution during inference on $\mathcal{D}_{\text{train}}$. To correct this, we need to fine-tune the BN layers of the backbone f on our training data $\mathcal{D}_{\text{train}}$, while keeping all other layers fixed. This fine-tuning will update the μ_{running} and σ_{running} to reflect the distribution of $\mathcal{D}_{\text{train}}$, aligning the activations with the intended standard normalization.

D. Limitations

A common limitation of our method can be that computational overhead introduced by graph creation (Sec. B.6). Future work could explore other graph-based approaches, such as GraphSAGE [10], which use neighborhood sampling to reduce computational costs. On the other hand, there is a trade-off between leveraging useful relational information by means of message passing and the risk of oversmoothing, which is a common issue in many graph-based approaches. We leave it to future work to introduce edgeweighted mechanisms and graph sampling techniques to address these potential limitations.

E. Code

Code to reproduce the results of our method is available at https://github.com/hdnugit/Graph_OOD_LTR.

Table 14. Ablation study for separate $\mathcal{D}_{\mathrm{out}}^{\mathrm{test}}$ for CIFAR10-LT as ID. The best and second-best results are bolded and underlined, respectively. Mean over six random runs are reported.

	Pre-						
$\mathcal{D}_{ ext{out}}^{ ext{test}}$	train	Gau.	GRL	Method	AUROC	AUPR	FPR95
	Х	Х	Х	Scratch (OE)	92.59	83.32	25.10
	Х	Х	1	Scratch+GCN	86.34	69.51	32.64
Т	1	Х	Х	Pre-train	94.42	90.58	26.77
Texture	1	Х	1	Pre-train+GCN	99.16	98.53	2.10
	1	1	Х	Pre-train+Gau.	96.58	94.49	19.23
	✓	1	1	Pre-train+Gau.+GCN (ours)	99.50	98.92	1.10
	Х	Х	Х	Scratch (OE)	95.10	97.14	16.15
	Х	Х	1	Scratch+GCN	87.67	91.66	32.16
SVHN	✓	Х	Х	Pre-train	97.00	98.71	15.64
SVIII	✓	Х	√	Pre-train+GCN	99.44	99.63	1.72
	✓	1	Х	Pre-train+Gau.	96.17	98.30	18.54
	√	1	√	Pre-train+Gau.+GCN (ours)	99.68	99.71	0.67
	Х	Х	Х	Scratch (OE)	83.40	80.93	56.96
	Х	Х	√	Scratch+GCN	79.55	73.12	56.27
CIFAR100	✓	Х	Х	Pre-train	84.13	83.90	57.24
CIFAR100	✓	Х	1	Pre-train+GCN	88.87	88.38	44.18
	√	1	Х	Pre-train+Gau.	85.92	86.48	55.13
	✓	1	√	Pre-train+Gau.+GCN (ours)	92.08	92.21	35.28
	Х	Х	Х	Scratch (OE)	86.14	79.33	47.78
	Х	Х	1	Scratch+GCN	81.75	70.13	44.80
TinyImageNet	✓	Х	Х	Pre-train	88.21	85.00	46.27
Tillylinagervet	✓	Х	✓	Pre-train+GCN	93.38	90.34	26.22
	✓	✓	Х	Pre-train+Gau.	90.20	88.02	42.69
	✓	1	✓	Pre-train+Gau.+GCN (ours)	95.61	93.64	19.93
	X	X	X	Scratch (OE)	91.35	87.62	27.86
	Х	Х	✓	Scratch+GCN	86.08	79.82	33.54
LSUN	✓	Х	X	Pre-train	93.26	92.88	31.92
LSOIT	✓	X	✓	Pre-train+GCN	<u>99.38</u>	<u>99.37</u>	1.88
	✓	1	Х	Pre-train+Gau.	94.30	94.40	30.40
	√	1	✓	Pre-train+Gau.+GCN (ours)	99.57	99.43	0.74
	Х	Х	Х	Scratch (OE)	90.07	95.15	34.04
	Х	Х	√	Scratch+GCN	84.09	90.98	35.92
Places365	✓	Х	Х	Pre-train	91.18	96.66	40.32
Traces303	✓	Х	√	Pre-train+GCN	<u>97.76</u>	99.09	9.55
	✓	✓	X	Pre-train+Gau.	92.37	97.25	38.36
	✓	1	√	Pre-train+Gau.+GCN (ours)	98.12	99.12	5.89
	Х	Х	Х	Scratch (OE)	89.77	87.25	34.65
	Х	Х	✓	Scratch+GCN	84.25	79.20	39.22
Average	✓	Х	Х	Pre-train	91.37	91.29	36.36
Tiverage	✓	Х	1	Pre-train+GCN	96.33	<u>95.89</u>	14.28
	✓	1	Х	Pre-train+Gau.	92.59	93.15	34.06
	√	1	✓	Pre-train+Gau.+GCN (ours)	97.43	97.17	10.60

Table 15. Ablation study for separate $\mathcal{D}_{\mathrm{out}}^{\mathrm{test}}$ for CIFAR100-LT as ID. The best and second-best results are bolded and underlined, respectively. Mean over six random runs are reported.

	Pre-						
$\mathcal{D}_{ ext{out}}^{ ext{test}}$	train	Gau.	GRL	Method	AUROC	AUPR	FPR95
	Х	Х	Х	Scratch (OE)	76.71	58.79	68.28
	Х	Х	1	Scratch+GCN	78.70	56.03	62.57
T	1	Х	Х	Pre-train	77.39	62.69	65.45
Texture	1	Х	1	Pre-train+GCN	88.70	81.86	46.35
	1	1	Х	Pre-train+Gau.	83.79	72.87	54.47
	✓	1	1	Pre-train+Gau.+GCN (ours)	90.88	84.10	39.32
	Х	Х	Х	Scratch (OE)	77.61	86.82	58.04
	Х	Х	1	Scratch+GCN	79.04	85.16	62.77
SVHN	1	Х	Х	Pre-train	83.80	91.15	49.25
SVIIIV	✓	Х	√	Pre-train+GCN	89.42	93.85	34.56
	✓	1	Х	Pre-train+Gau.	91.65	95.90	33.24
	✓	1	√	Pre-train+Gau.+GCN (ours)	97.02	98.19	10.19
	X	Х	X	Scratch (OE)	62.23	57.57	80.64
CIFAR10 X	Х	Х	√	Scratch+GCN	64.98	59.53	78.15
	✓	Х	Х	Pre-train	64.02	60.22	80.23
	✓	Х	1	Pre-train+GCN	72.80	68.96	71.20
	✓	1	Х	Pre-train+Gau.	68.99	66.00	77.65
	✓	1	√	Pre-train+Gau.+GCN (ours)	75.08	74.17	70.62
	Х	Х	Х	Scratch (OE)	68.04	51.66	76.66
	Х	Х	√	Scratch+GCN	68.37	51.73	77.60
TinyImageNet	✓	Х	Х	Pre-train	71.47	56.95	74.29
Tillytillagervet	✓	Х	✓	Pre-train+GCN	75.73	62.25	69.33
	✓	✓	Х	Pre-train+Gau.	74.70	61.74	70.48
	✓	1	✓	Pre-train+Gau.+GCN (ours)	80.06	68.96	63.48
	X	X	X	Scratch (OE)	77.10	61.42	63.98
	Х	Х	✓	Scratch+GCN	76.26	57.55	65.52
LSUN	✓	Х	X	Pre-train	65.18	53.89	81.17
LSON	✓	X	✓	Pre-train+GCN	<u>79.14</u>	69.66	69.21
	✓	1	Х	Pre-train+Gau.	72.06	62.26	77.96
	✓	✓	√	Pre-train+Gau.+GCN (ours)	83.29	75.09	59.57
	Х	Х	Х	Scratch (OE)	75.80	86.68	65.72
	Х	Х	√	Scratch+GCN	76.26	85.78	64.88
Places365	✓	Х	Х	Pre-train	71.18	85.69	77.00
Traces303	✓	Х	√	Pre-train+GCN	82.57	91.73	62.65
	✓	✓	X	Pre-train+Gau.	76.89	89.04	70.86
	✓	1	1	Pre-train+Gau.+GCN (ours)	84.22	92.63	58.87
	Х	Х	Х	Scratch (OE)	72.91	67.16	68.89
	Х	Х	✓	Scratch+GCN	73.93	65.97	68.58
Average	✓	Х	Х	Pre-train	72.17	68.43	71.23
	✓	Х	1	Pre-train+GCN	81.40	<u>78.05</u>	58.88
	√	1	Х	Pre-train+Gau.	78.01	74.64	64.11
	✓	1	1	Pre-train+Gau.+GCN (ours)	85.09	82.19	50.34